Computational Mechanics (1992) 10, 369–379

Computational Mechanics

An adaptive mesh refinement technique for the analysis of shear bands in plane strain compression of a thermoviscoplastic solid

R. C. Batra and **K.-I. Ko**

Department of Mechanical and Aerospace Engineering and Engineering Mechanics, University of Missouri–Rolla, Rolla, MO 65401-0249, USA

Abstract. We have developed an adaptive mesh refinement technique that generates elements such that the integral of the second invariant of the deviatoric strain-rate tensor over an element is nearly the same for all elements in the mesh. It is shown that the finite element meshes so generated are effective in resolving shear bands, which are narrow regions of intense plastic deformation that form in high strain-rate deformation of thermally softening viscoplastic materials. Here we assume that the body is deformed in plane strain compression at a nominal strain-rate of 5000 $\sec^{-1}$, and model a material defect by introducing a temperature perturbation at the center of the block.

1 Introduction

In nearly all of the previous numerical studies of shear bands in two-dimensional problems involving a viscoplastic material (e.g., see Needleman 1989; Batra and Liu 1989; Batra and Zhu 1991), a fixed finite element mesh has been used. Since shear bands are narrow regions of intense plastic deformation, their satisfactory resolution requires either a very fine mesh throughout the computational domain, in which case the solution in most of the domain outside the shear band is overcomputed, or an adaptively refined mesh that concentrates more elements in the severely deforming region and fewer elements outside of it. Batra and Kim (1990) developed an adaptive mesh refinement technique for the analysis of one-dimensional shear banding problems by ensuring that the scaled residuals of the equations expressing the balance of linear momentum and the balance of internal energy were uniformly distributed. They subdivided elements having large scaled residuals and observed that high values of the scaled residuals occurred, in general, in non-overlapping regions. Their technique did not combine elements with low values of the scaled residuals, and for this reason did not result in an optimum mesh. We make no attempt to review all of the literature on adaptive mesh refinement and two-dimensional adiabatic shear banding problems. For the former, we refer the reader to Safjan et al. (1991) and Zienkiewicz and Zhu (1991), and for the latter to Batra and Zhu (1991).

2 Formulation of the problem

We use a fixed set of rectangular Cartesian coordinates with origin at the centroid of a square block (cf. Fig. 1) to analyze its plane strain thermomechanical deformations. We assume that the block is made of a thermally softening viscoplastic material. In terms of the referential description, governing equations are:

$$(\rho J)^{\cdot} = 0, \qquad \rho_0 \dot{v}_i = T_{i\alpha,\alpha}, \qquad \rho_0 \dot{e} = -Q_{\alpha,\alpha} + T_{i\alpha} v_{i,\alpha}, \tag{1–3}$$

where

$$J = \det F_{i\alpha}, \quad F_{i\alpha} = x_{i,\alpha}, \quad x_{i,\alpha} = \partial x_i / \partial X_\alpha, \tag{4}$$

x_i is the present location of a material particle that occupied place X_α in the reference configuration,

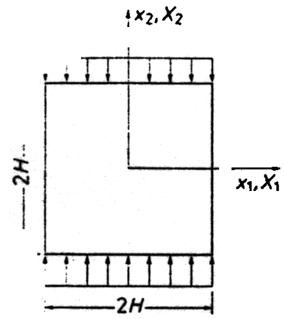

Fig. 1. A schematic sketch of the problem studied

ρ its present mass density, ρ_0 its mass density in the reference configuration, v_i its present velocity, $T_{i\alpha}$ the first Piola–Kirchoff stress tensor, Q_α the heat flux per unit reference area, e the specific energy, a superimposed dot indicates the material time derivative, and a repeated index implies summation over the range of the index. For the constitutive relations we take

$$\sigma_{ij} = -B\left(\frac{\rho}{\rho_0} - 1\right)\delta_{ij} + 2\mu D_{ij}, \qquad T_{i\alpha} = \frac{\rho_0}{\rho} X_{\alpha,j}\sigma_{ij} \tag{5.1, 5.2}$$

$$2\mu = \frac{\sigma_0}{\sqrt{3}I}(1 + bI)^m(1 \quad \nu\theta) \tag{6}$$

$$2D_{ij} = v_{i,j} + v_{j,i}, \qquad 2I^2 = \bar{D}_{ij}\bar{D}_{ij}, \qquad \bar{D}_{ij} = D_{ij} \quad \tfrac{1}{3}D_{kk}\delta_{ij} \tag{7.1–7.3}$$

$$Q_\alpha = \frac{\rho_0}{\rho} X_{\alpha,j} q_j, \qquad q_i = \quad k\theta_{,i} \tag{8.1, 8.2}$$

$$\dot{e} = c\dot{\theta} + B\left(\frac{\rho}{\rho_0} - 1\right)\frac{\dot{\rho}}{(\rho_0\rho)}. \tag{9}$$

Here σ_{ij} is the Cauchy stress tensor, B may be thought of as the bulk modulus for the material of the block, $\mathbf{D}$ is the strain-rate tensor, σ_0 the yield stress of the material in a quasistatic simple tension or compression test, parameters b and m characterize the strain-rate sensitivity of the material, I is the second invariant of the deviatoric strain-rate tensor $\bar{\mathbf{D}}$, ν is the coefficient of thermal softening, k equals the thermal conductivity of the material, c the specific heat, and θ the temperature rise of a material particle.

We introduce non-dimensional variables, indicated below by a superimposed bar, as follows.

$$\begin{aligned} &\bar{t} = t\dot{\gamma}_0, \quad \bar{I} = I/\dot{\gamma}_0, \quad \bar{b} = b\dot{\gamma}_0, \quad \bar{\rho} = \rho/\rho_0, \quad \bar{\boldsymbol{\sigma}} = \boldsymbol{\sigma}/\sigma_0, \quad \bar{\mathbf{T}} = \mathbf{T}/\sigma_0, \\ &\bar{B} = B/\sigma_0, \quad \bar{\nu} = \nu\theta_r, \quad \bar{\theta} = \theta/\theta_r, \quad \bar{\boldsymbol{v}} = \boldsymbol{v}/v_0, \quad \bar{\boldsymbol{x}} = \boldsymbol{x}/H, \quad \bar{\boldsymbol{X}} = \boldsymbol{X}/H, \\ &\delta = \rho_0 v_0^2/\sigma_0, \quad \beta = k/(\rho_0 c v_0 H), \end{aligned} \tag{10a}$$

where

$$\theta_r \equiv \sigma_0/(\rho_0 c), \quad \dot{\gamma}_0 \equiv v_0/H. \tag{10b}$$

In Eq. (10) $2H$ is the height of the square block, θ_r the reference temperature, v_0 is the steady value of the velocity applied to the top and bottom surfaces in the x_2-direction, and $\dot{\gamma}_0$ equals the average applied strain-rate. Henceforth we use non-dimensional variables and drop the superimposed bars. We presume that the deformations of the block are symmetrical about the horizontal and vertical centroidal axes, and study the deformations of the material in the first quadrant.

For the boundary conditions we take

$$v_2 = 0, \quad T_{12} = 0, \quad Q_2 = 0 \quad \text{on} \quad x_2 = X_2 = 0, \tag{11.1}$$

$$v_1 = 0, \quad T_{21} = 0, \quad Q_1 = 0 \quad \text{on} \quad x_1 = X_1 = 0, \tag{11.2}$$

$$T_{11} = 0, \quad T_{21} = 0, \quad Q_1 = 0 \quad \text{on} \quad X_1 = H, \tag{11.3}$$

$$v_2 = -h(t), \quad T_{12} = 0, \quad Q_2 = 0 \quad \text{on} \quad X_2 = H. \tag{11.4}$$

The boundary conditions (11) signify that the boundaries of the block are insulated, the right surface is traction free, there is no tangential traction acting on the top surface, and the top surface moves downward at a prescribed speed $h(t)$. The boundary conditions (11.1) and (11.2) follow from the assumed symmetry of deformations about the X_1 and X_2 axes.

For the initial conditions we take

$$\rho(x,0) = 1, \quad v_1(x,0) = 0.37x_1, \quad v_2(x,0) = -x_2, \tag{12.1–12.3}$$

$$\theta(x,0) = 0.2(1-r^2)^9 e^{-5r^2}, \quad r^2 = X_1^2 + X_2^2. \tag{12.4, 12.5}$$

The initial conditions on the velocity field represent the situation when the transients have died out. Batra and Liu (1989) found this velocity field by taking

$$\begin{aligned} h(t) &= t/0.005, \quad 0 \leqq t \leqq 0.005, \\ &= 1, \qquad\qquad t \geqq 0.005, \end{aligned}$$

assuming that the initial temperature distribution is uniform, and computing the solution till the steady state had been reached. The changes in the mass density and the computed temperature rise were found to be insignificant to justify assuming that the initial mass density is uniform. The assumptions (12.2) and (12.3) result in a smaller value of the CPU time needed to analyze the problem and do not affect the qualitative nature of the results. The initial temperature distribution given by (12.4) models a material inhomogeneity; the amplitude of the perturbation can be thought of as representing the strength of the singularity.

Equations obtained by combining (1) through (9) are to be solved under the side conditions (11) and (12). Since these coupled equations are highly nonlinear, it is not clear whether or not they have a unique solution. Here we find their approximate solution by first reducing the partial differential equations to a set of coupled, nonlinear, and ordinary stiff differential equations by using the Galerkin approximation. The number of these equations equals four times the number of nodes in the finite element discretization of the domain. We use three-noded isoparametric triangular elements and the lumped mass matrix obtained by the row-sum technique. These stiff ordinary differential equations are integrated with respect to time by using the backward difference Adam's method included in the subroutine LSODE (e.g., see Hindmarsh 1971). We could not use the Gear method because of the limited core storage available to us. The computer code developed by Batra and Liu (1989) was suitably modified to solve the present problem.

3 Adaptive mesh refinement technique

We first select a coarse mesh and find a solution of the aforestated problem. This mesh is refined so that

$$a_e = \int_{\Omega_e} I \, d\Omega, \quad e = 1, 2, \ldots, n_{el}, \tag{13}$$

is nearly the same for each element Ω_e. In (13), n_{el} equals the number of elements in the coarse mesh and Ω_e is one of the elements. Since one may not have an idea where the solution will exhibit sharp gradients, we choose the coarse mesh to be uniform. The motivation behind making a_e the same over each element Ω_e is that within the region of localization of the deformation values of I are very high as compared to those in the remaining region. Other variables such as the temperature rise, the maximum principal strain, and the equivalent strain which are also quite large within the band will be suitable replacements for I in Eq. (13). The refined mesh will depend upon the variable used in Eq. (13). In order to refine the mesh, we find

$$\bar{a} = \frac{1}{n_{el}} \sum_{e=1}^{n_{el}} a_e, \quad \xi_e = \frac{a_e}{\bar{a}}, \quad h_e = \frac{\bar{h}_e}{\xi_e}, \quad \text{and} \quad H_n = \frac{1}{N_e} \sum_{e=1}^{N_e} h_e, \quad n = 1, 2, \ldots, n_{od}. \tag{14–17}$$

Here, $\bar{h}_e$ is the size of the element Ω_e in the coarse mesh, N_e equals the number of elements meeting at node n, and n_{od} equals the number of nodes in the coarse mesh. We refer to H_n as the nodal element size at node n.

In order to generate the new mesh, we first discretize the boundary by following the procedure given by Cescotto and Zhou (1989). Let AB be a segment of the contour to be discretized, s the arc length measured from point A, and H_A and H_B be nodal element sizes for nodes located at points A and B, respectively. From a knowledge of the values of H at discrete points, corresponding to the nodes in the coarse mesh, on AB we define a piecewise linear continuous function $H(s)$ that takes the previously computed values at the node points. In order to discretize AB for the new mesh, we start from point A if $H_A < H_B$; otherwise we start from B. For the sake of discussion, let us assume that A is the starting point. We first find temporary positions of nodes on the segment AB by using the following recursive procedure. Assume that points $1, 2, \ldots, k$ have been found. Then the temporary location of point $(k+1)$ is given by

$$s_{k+1} = s_k + \tfrac{1}{2}[H(s_k) + H(s^*_{k+1})], \tag{18}$$

where

$$s^*_{k+1} = s_k + H(s_k). \tag{19}$$

Referring to Fig. 2, the above procedure will give rise to the following four alternatives: $a = b = 0$, $a < b$, $a > b$, $a = b \neq 0$. If $a = b = 0$, then the temporary locations of node points are their final positions. Depending upon whether $a < b$ or $b \leqq a$, the node points 2 to p or 2 to $p+1$ are moved, the displacement of a node being proportional to the value of H there, so that either node p or node $(p+1)$ coincides with B. This determines the final positions of nodes on the segment AB.

Having discretized the boundary, we use the concept of advancing front (e.g., see Lo 1985; Peraire et al. 1987, 1988; Habraken and Cescotto 1990) to generate the elements. An advancing front consists of straight line segments which are available to form a side of an element. Thus, to start with, it consists of the discretized boundary. We choose the smallest line segment (say side AB) connecting the two adjoining nodes, and determine the nodal element size $H_M \equiv H(s_M) = (H_A + H_B)/2$ at the midpoint M of AB. We set

$$\delta \quad \begin{cases} 0.8\,\overline{AB} & \text{if} \quad H_M < 0.8\,\overline{AB}, \\ H_M & \text{if} \quad 0.8\,\overline{AB} \leqq H_M \leqq 1.4\,\overline{AB}, \\ 1.4\,\overline{AB} & \text{if} \quad 1.4\,\overline{AB} < H_M, \end{cases}$$

and find point C_1 at a distance δ from A and B (cf. Fig. 3). Here $\overline{AB}$ equals the length of segment AB. We search for all nodes on the active front that lie inside the circle with center at C_1 and

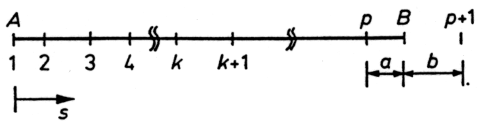

Fig. 2. Discretization of a boundary segment for mesh refinement

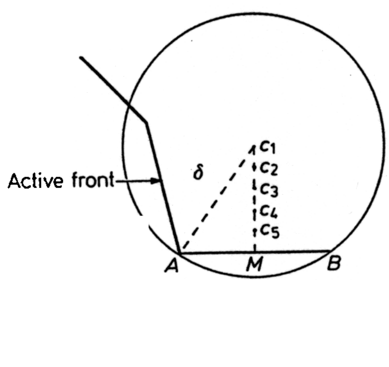

Fig. 3. Advancing front and new element generation

radius δ, and order them according to their distance from C_1 with the first node in the list being closest to C_1. At the end of this list are added points C_1, C_2, C_3, C_4, and C_5, which lie on C_1M and divide it into five equal parts. We next determine the first point C in the list that satisfies the following three conditions.

(i) Area of triangle ABC > 0.
(ii) Sides AC and BC do not cut any of the existing sides in the front.
(iii) If any of the points $C_1, C_2, \ldots, C_5$ is chosen, that point is not too close to the front.

The triangle ABC is an element in the new mesh. If C is one of the points $C_1, C_2, \ldots, C_5$, then a new node is also created. The advancing front is updated by removing the line segment AB from it, and adding line segments AC and CB to it. The element generation process ceases when there is no side left in the active front.

We determine the values of solution variables at a newly created node by first finding out to which element in the coarse mesh this node belongs, and then finding values of solution variables at this node by interpolation. This process and that of searching for line segments and points in the aforestated element generation technique consume a considerable amount of CPU time. These operations are optimized to some extent by using the heap list algorithm (e.g., see Löhner, 1988) for deleting and inserting new line segments, and quadtree structures and linked lists for searching line segments and points and also for the interpolation of solution variables at the newly created nodes.

4 Results and discussion

We assume that the block is made of a typical steel and assign the following values, also used by Batra and Liu (1989), to various parameters.

$$\begin{aligned}&b = 10{,}000\,\text{sec}, \quad \sigma_0 = 333\,\text{MPa}, \quad k = 49.2\,\text{W}\,\text{m}^{-1}\,{}^\circ\text{C}^{-1}, \quad m = 0.025, \quad c = 473\,\text{J}\text{kg}^{-1}\,{}^\circ\text{C}^{-1},\\ &\quad \rho_0 = 7{,}800\,\text{kg/m}^3, \quad \text{B} = 128\,\text{GPa}, \\ &v = 0.0222\,{}^\circ\text{C}^{-1}, \quad v_0 = 25\,\text{m}\,\text{sec}^{-1}, \quad H = 5\,\text{mm}, \quad h(t) = 1.0.\end{aligned} \tag{21}$$

Here we have made an exception to our notation and indicated dimensional quantities to clarify the units used. As stated earlier, the transients are assumed to have died out, the top surface moves downward with the prescribed speed v_0, and the average strain-rate at which the block is being deformed equals $5000\,\text{sec}^{-1}$. For values given in (21), $\theta_r = 89.6\,{}^\circ$C, and the non-dimensional melting temperature equals 0.5027. We note that the value of the thermal softening coefficient v has been purposely taken to be high so as to reduce the computational time. It should not affect the qualitative nature of the results reported herein. The test data to find values of material parameters at strain-rates, strains, and temperatures likely to occur in a shear band is not available.

Figure 4 depicts the initial coarse mesh at time $t = 0$, and the generated refined meshes at non-dimensional time $t = 0.025$, 0.040, and 0.047. We note that the non-dimensional time also equals the average strain. In the solution of the problem, the mesh was also adaptively refined at $t = 0.015$, 0.030, and 0.035; however, these are not shown here for the sake of brevity. The times at which the mesh is refined were selected manually, and are to some degree arbitrary. A possible criterion could be to refine the mesh when the second invariant of the strain-rate tensor or the temperature at the center has risen by a certain amount. The meshes shown in Fig. 4 vividly reveal that the refinement technique outlined in Sect. 3 gives rise to nonuniform meshes with finer mesh in the severely deforming region and coarse mesh elsewhere. We did not impose any restriction on the number of new nodes that can be introduced when the mesh is refined. Practical considerations such as the core storage available may require this kind of restriction.

In Fig. 5 we have plotted the contours of the second invariant I of the deviatoric strain-rate tensor at $t = 0.019$, 0.032, 0.042, and 0.047 in the deformed configuration. These plots suggest that as the block continues to be deformed, the deformation localizes into a band whose width keeps on decreasing. Contours of successively increasing values of I originate from the center of the block and propagate outward. The contours of the temperature rise at $t = 0.019$, 0.032, 0.042, and 0.047

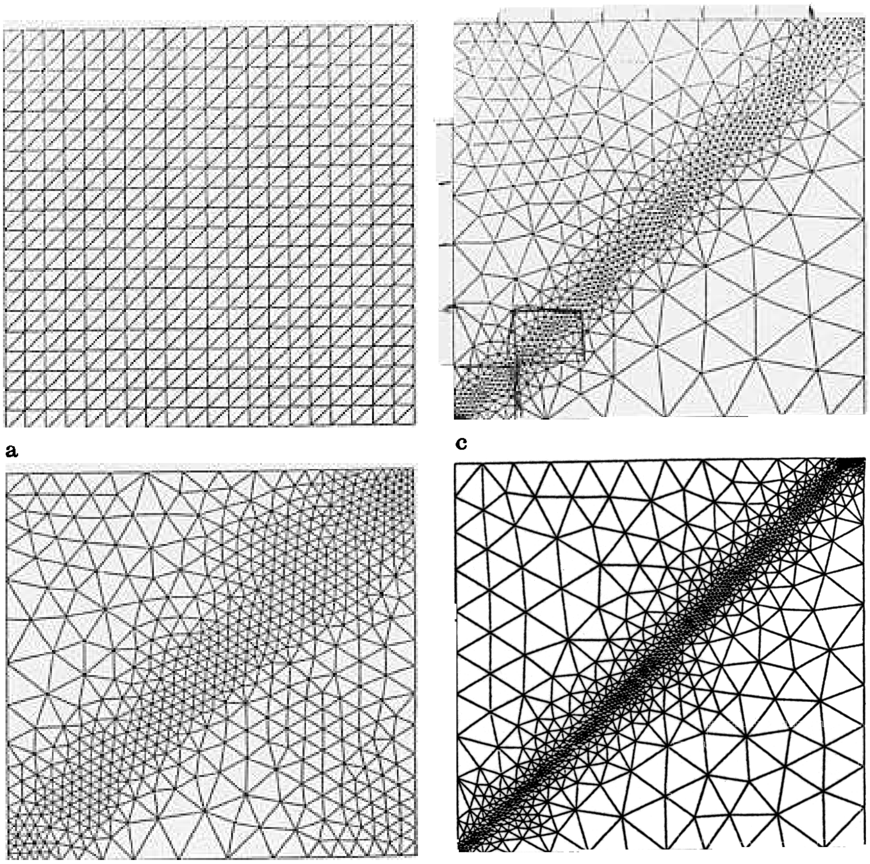

a c b d

Fig. 4 a–d. Finite element meshes at **a** $t = 0.0$, **b** $t = 0.025$, **c** $t = 0.040$, and **d** $t = 0.047$

are exhibited in Fig. 6. The distribution of the velocity field in the deforming region at $t = 0.047$ is shown in Fig. 7. These plots support Tresca's (1878) and Massey's (1921) assertions that the tangential velocity is discontinuous across a shear band. In our work the velocity field is forced to be continuous throughout the domain. The sharp jumps in v_1 and v_2 across the shear band lend credence to the discontinuity of the tangential velocity across the shear band. The plot of the effective stress s_e, defined as

$$s_e = \sqrt{\tfrac{2}{3}}(1 - v\theta)(1 + bI)^m,$$

in Fig. 8 reveals that s_e drops considerably within the shear band. All of the aforestated observations are in qualitative agreement with Batra and Liu's (1989) results, except that the results reported herein are sharper in the sense that the region of localized deformation is considerably narrower and the computed values of I_{max} for the same value of θ_{max} are higher. Here I_{max} and θ_{max} denote, respectively, the peak values of the second invariant of the deviatoric strain-rate tensor and the temperature rise. For example, at $\theta_{max} = 0.45$, Batra and Liu (1989) found $I_{max} = 21$. Here, we get $I_{max} = 91$ for the same value of θ_{max}. We note that Batra and Liu (1989) used 9-noded quadrilateral elements and employed a fixed 16×16 mesh.

In an attempt to elucidate the improvement, if any, in the computed results obtained by using adaptively refined meshes, we have plotted in Fig. 9 the evolution, at the block center, of the second invariant I of the deviatoric strain-rate tensor, the temperature rise, and the effective stress for three different meshes. Two of these meshes with 441 and 841 nodes, and consisting of uniform linear triangular elements are fixed, while the third one was adaptively refined at times $t = 0.015$, 0.025, 0.030, 0.035, 0.040, and 0.047 with uniform linear triangular elements and 441 nodes at $t = 0$

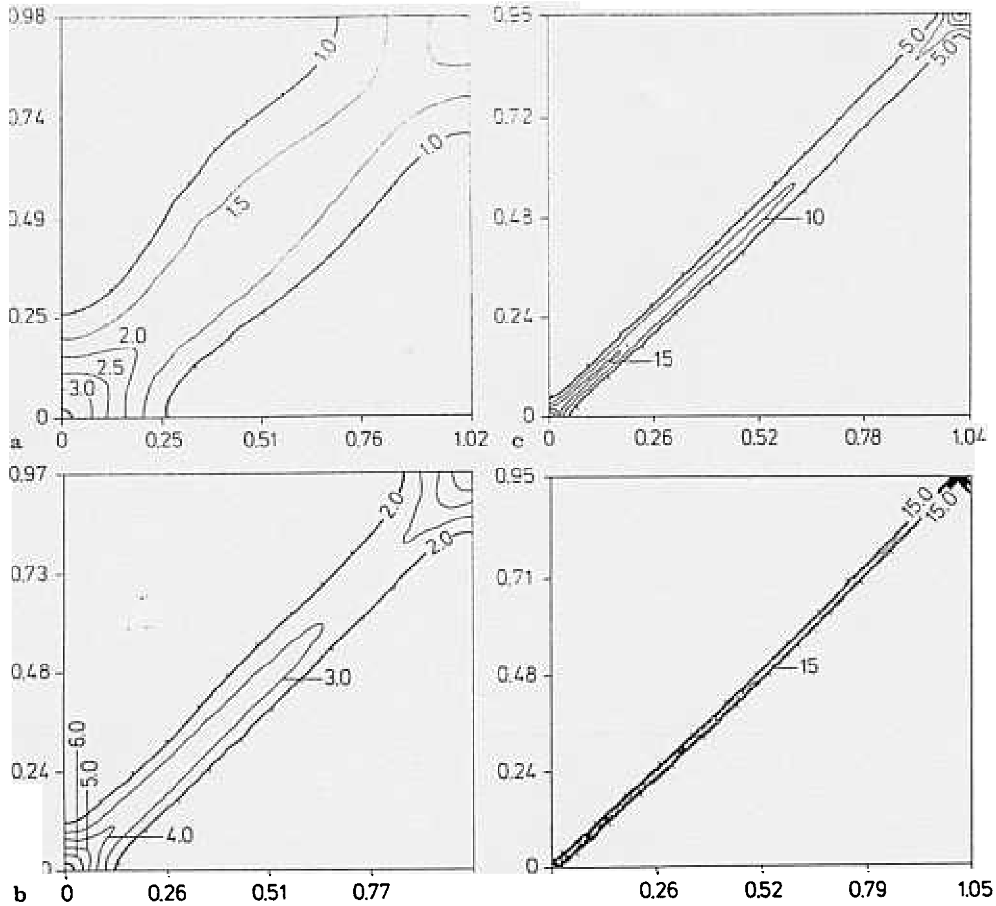

Fig. 5 a–d. Contours of the second invariant of the deviatoric strain-rate tensor at **a** $t = 0.019$, **b** $t = 0.032$, **c** $t = 0.042$, and **d** $t = 0.047$

and nonuniform linear triangular elements with 1200 nodes at $t = 0.047$. Out of the three variables s_e, I, and θ, the evolution of I is affected most by the successive refinements of the mesh. For the two fixed meshes with 441 and 841 nodes, I at the specimen center seems to reach a plateau, which is misleading. Also after the deformation has started to localize, the temperature rise and its rate of increase are higher for the adaptively refined mesh than those for either of the other two fixed meshes. For the solution with the adaptively refined mesh, I at the block center increases from 10 at $\gamma_{avg} = 0.035$ to nearly 52 at $\gamma_{avg} = 0.045$, giving a rate of increase of strain-rate of $10^{11}\ \text{sec}^{-2}$. If one assumes that the deformation begins to localize earnestly at $\gamma_{avg} = 0.035$, then the generalized strain, defined as $\int I\,dt$, at the block center increases by 0.3 in two microseconds. The larger drop in s_e in spite of the sharp increase in the value of I indicates that thermal softening dominates over the strain-rate hardening effects. It is due to the rather high value of the thermal softening coefficient ν used here. Note that increasing the value of nondimensional I from 10 to 100 changes the value of $(1 + bI)^m$ from 1.65 to 1.75.

We now investigate the change, if any, in the approximate solution caused by refining the mesh. This task would be easy if the analytical solution of the problem were known. Since such is not the case and there is little hope of finding an analytical solution of the problem in the near future, we compare our approximate solution with a higher-order approximate solution (Hinton and Campbell, 1974) obtained by smoothening out the computed solution. Let g be one of the solution variables to be smoothened. For the three-noded triangular element, we write

$$g(\xi, \eta) = a\xi + b\eta + c, \tag{23}$$

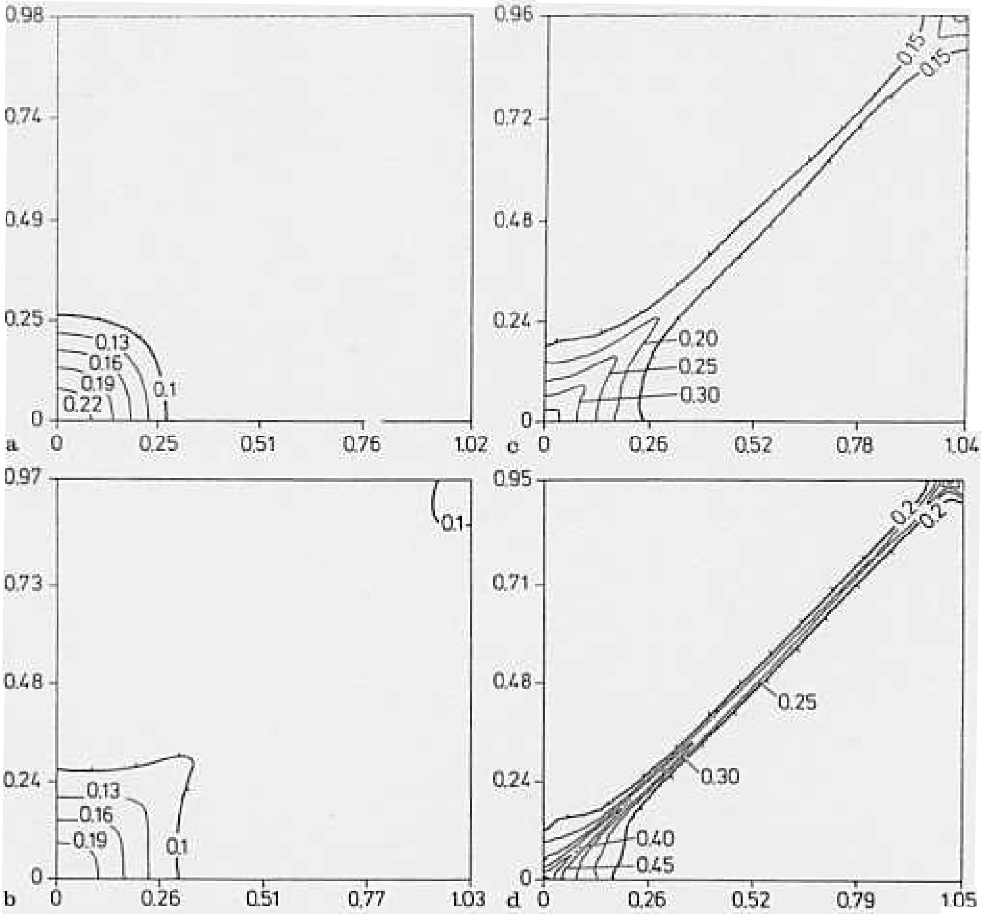

Fig. 6 a–d. Contours of the temperature rise at a $t = 0.019$, b $t = 0.032$, c $t = 0.042$, and d $t = 0.047$

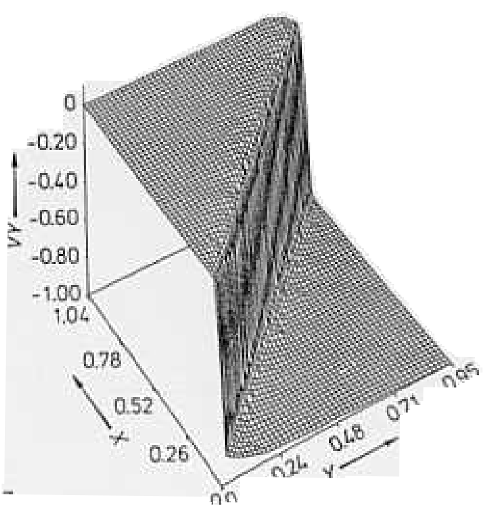

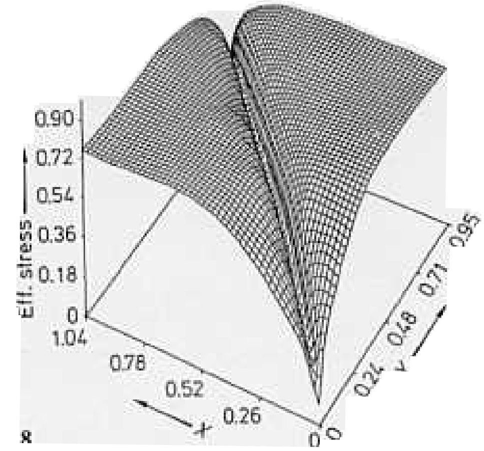

Figs. 7 and 8. Distribution 7 of the velocity field at $t = 0.047$, and 8 of the effective stress at $t = 0.047$

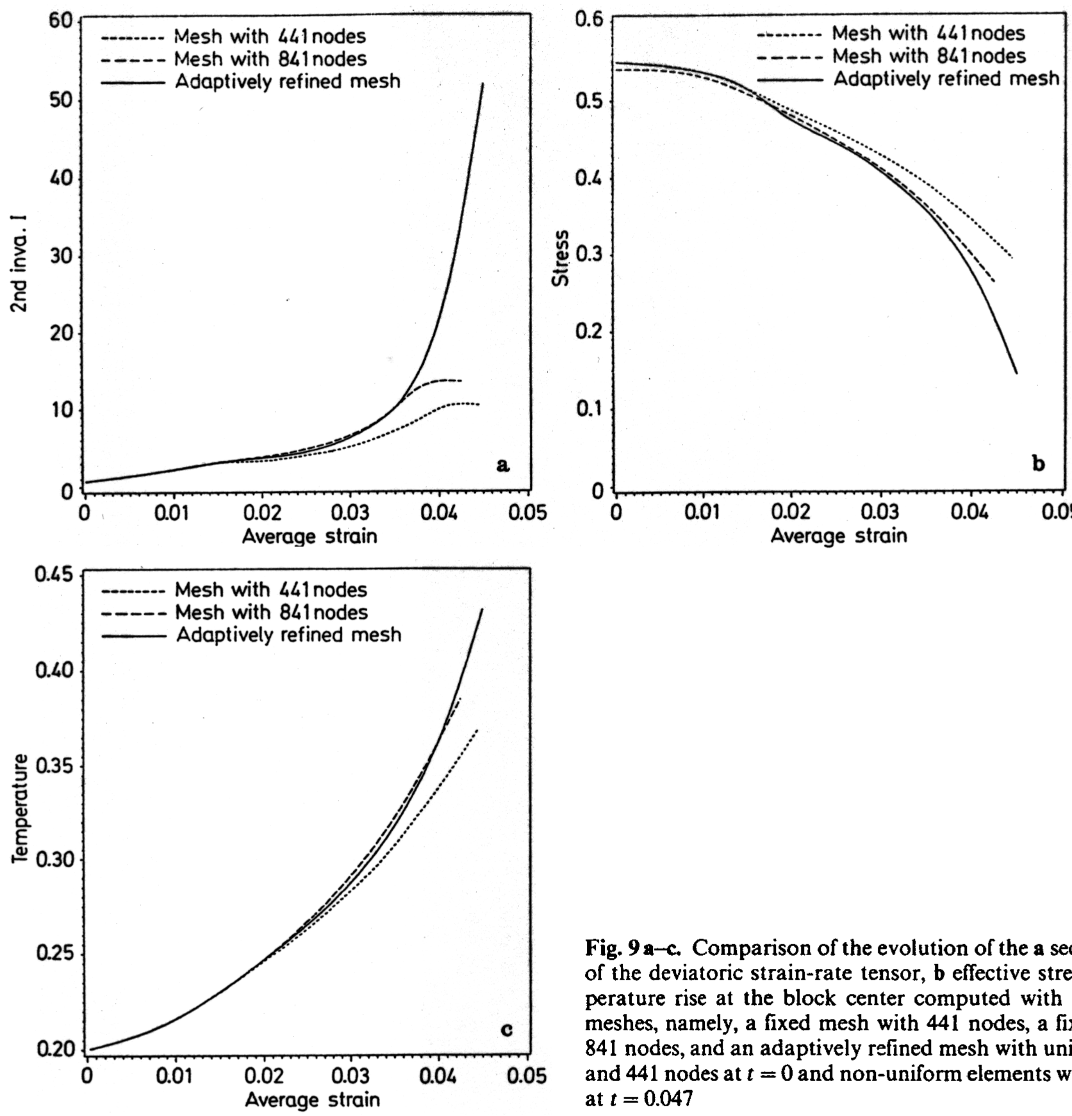

Fig. 9 a–c. Comparison of the evolution of the **a** second invariant of the deviatoric strain-rate tensor, **b** effective stress, and **c** temperature rise at the block center computed with three different meshes, namely, a fixed mesh with 441 nodes, a fixed mesh with 841 nodes, and an adaptively refined mesh with uniform elements and 441 nodes at $t = 0$ and non-uniform elements with 1200 nodes at $t = 0.047$

where ξ and η are area coordinates of a point, and constants a, b, and c are determined from the values of g at three quadrature points located within the triangular element. From (23) we can evaluate g at the vertices of the triangle. Then the value g_n^* of the smoothened solution at a node n is given by

$$g_n^* = \frac{1}{N_e} \sum_{n=1}^{N_e} g_n, \tag{24}$$

where N_e equals the number of elements sharing the node n, and the summation sign on the right-hand side implies the sum of the values of g at node n evaluated for each element meeting at that node. Knowing g^* at each node, we can interpolate its value at any other point by using the finite element basis functions. We define the percentage error η in the deviatoric strain-rate tensor $\bar{\mathbf{D}}$ by the relation

$$\eta = \left(\frac{\|\mathbf{e}\|_0^2}{\|\mathbf{e}\|_0^2 + \|\bar{\mathbf{D}}\|_0^2} \right)^{1/2} \times 100, \tag{25}$$

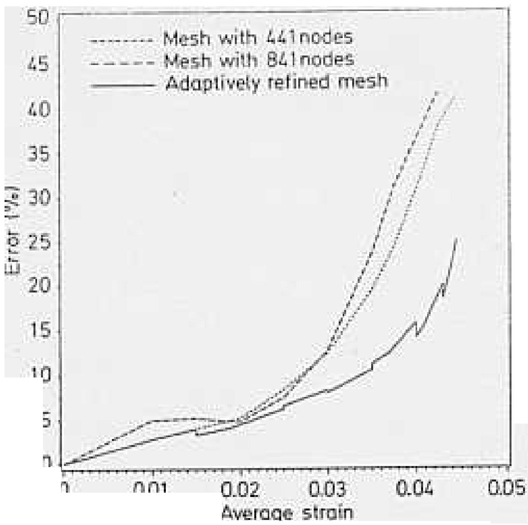

Fig. 10. Comparison of the error in the computed approximate solution and the higher-order approximate solution for three different meshes; fixed mesh with 441 nodes, fixed mesh with 841 nodes, and an adaptively refined mesh

where

$$\mathbf{e} = \bar{\mathbf{D}} - \bar{\mathbf{D}}^*, \qquad \|\mathbf{e}\|_0^2 = \sum_{e=1}^{N_{el}} \int_{\Omega_e} \mathbf{e}^T \mathbf{e} \, d\Omega, \tag{26.1, 26.2}$$

and N_{el} equals the number of elements in the mesh. The plot of the percentage error η in Fig. 10 for the three meshes shows that the error is lower for the approximate solution obtained by using the adaptively refined mesh as compared to the other two meshes. That the error measure is rather crude is indicated by the slightly larger errors obtained with a fixed mesh of 841 nodes as compared to that with 441 nodes. It could be due to the larger errors caused by smoothening out of the approximate solution with 841 nodes since the band in this case is more intense than that for the mesh with 441 nodes.

5 Conclusions

We have used adaptively refined meshes to study the initiation and growth of shear bands in a square block made of a viscoplastic material. The mesh is refined at various times to ensure that the integral of the second invariant of the deviatoric strain-rate tensor over each element is nearly the same for all elements in the mesh. It generates a non-uniform mesh with small elements in regions where the strain-rate is high and large elements elsewhere. It is shown that such meshes are quite effective in analyzing problems in which the deformation localizes into narrow bands of intense plastic deformation. A comparison of the computed solution with a higher-order approximate solution reveals that the use of the adaptively refined meshes leads to lower error in the approximate solution as compared to that obtained with a fixed mesh. For the problem studied herein, the band forms in about two microseconds, and at a homologous temperature of 0.99 at the specimen center, the maximum strain-rate there equals $4.65 \times 10^5 \text{ sec}^{-1}$.

Acknowledgements

This work was supported by the U.S. Army Research Office Grant DAAL03-91-G-0084 and the U.S. NSF grant M SS-9121279 to the University of Missouri–Rolla. Some of the computations were performed on the NSF sponsored supercomputer center in Ithaca, NY.

References

Batra, R. C.; Liu, D.-S. (1989): Adiabatic shear banding in plane strain problems. J. Appl. Mech. 56, 527–534

Batra, R. C.; Zhu, Z. G. (1991): Dynamic shear band development in a bimetallic body containing a void. Int. J. Sol. Struct. 27, 1829–1854

Cescotto, S.; Zhou, D. W. (1989): A variable density mesh generation for planar domains. Comm. Appl. Num. Meth. 5, 473–481

Habraken, A. M.; Cescotto, S. (1990): An automatic remeshing technique for finite element simulation of forming processes. Int. J. Num. Meth. Eng. 30, 1503–1525

Hindmarsh, A. C. (1983): ODEPACK, A systematized collection of ODE solvers. In: Stepleman, R. S. et al. (eds): Scientific computing, pp 55–64. Amsterdam, North-Holland

Hinton, E.; Campbell, J. S. (1974): Local and global smoothing of discontinuous finite element functions using a least squares method. Int. J. Num. Meth. Eng. 8, 461–480

Lo, S. H. (1985): A new mesh generation scheme for arbitrary planar domains. Int. J. Num. Meth. Eng. 21, 1403–1426

Löhmer, R. (1988): Some useful data structures for the generation of unstructured grids. Comm. Appl. Num. Meth. 4, 123–135

Massey, H. F. (1921): The flow of metal during forging. Proc. Manchester Assoc. Engrs. 21–26

Needleman, A. (1989): Dynamic shear band development in plane strain. J. Appl. Mech. 56, 1–9

Peraire, J.; Vahdati, M.; Morgan, K.; Zienkiewicz, O. C. (1987): Adaptive remeshing for compressible flow computations J. Comp. Phys. 72, 449–466

Peraire, J.; Peiro, J.; Formaggia, L.; Horgan, K.; Zienkiewicz, O. C. (1988): Finite element Euler computations in three dimensions. Int. J. Num. Meth. Eng. 26, 2135–2159

Safjan, A.; Demkowicz, L.; Oden, J. T. (1991): Adaptive finite element methods for hyperbolic systems with application to transient acoustics. Int. J. Num. Meth. Eng. 32, 677–707

Tresca, H. (1878): On further application of the flow of solids. Proc. Inst. Mech. Eng. 30, 301–345

Zienkiewicz, O. C.; Zhu, J. Z. (1991): Adaptivity and mesh generation. Int. J. Num. Meth. Eng. 32 783–810

Communicated by S. N. Atluri, February 11, 1992